Overcoming the Dipolar Disorder in Dense CoFe Nanoparticle Ensembles: Superferromagnetism

S. Bedanta,[1] T. Eimüller,[2] W. Kleemann,[1,*] J. Rhensius,[1] F. Stromberg,[1] E. Amaladass,[3] S. Cardoso,[4] and P. P. Freitas[4]

[1]*Angewandte Physik, Universität Duisburg-Essen, 47048 Duisburg, Germany*
[2]*Nachwuchsgruppe Magnetische Mikroskopie, Ruhr-Universität Bochum, 44780 Bochum, Germany*
[3]*Max-Planck-Institut für Metallforschung, 70569 Stuttgart, Germany*
[4]*INESC, Rua Alves Redol 9-1, 1000 Lisbon, Portugal*

(Received 25 September 2006; published 25 April 2007)

In a dense ensemble of physically nonpercolating FM nanoparticles embedded in a $[Co_{80}Fe_{20}/Al_2O_3]_{10}$ multilayer the long-discussed superferromagnetic (SFM) state has been evidenced by imaging homogeneously magnetized SFM domain patterns with x-ray photoemission electron microscopy and magneto-optical Kerr microscopy. Competing dipolar and exchange interactions give rise to extremely rough domain walls similarly as in hard multigrain magnets. The SFM state is characterized by extreme magnetic softness and higher order tunneling conductivity due to atomically small intercalated particles promoting the SFM order.

DOI: 10.1103/PhysRevLett.98.176601 PACS numbers: 72.25.Ba, 75.60.Jk, 75.70.−i, 75.75.+a

Recent developments in microelectronic devices, spintronics [1], and high density magnetic recording heads have increased the demand for further miniaturization and higher frequency operation of magnetic devices. In particular, soft magnetic thin films with high permeability, μ, and low eddy current losses are required for high frequencies, f. To this end materials with excellent μ-f response should have high electrical resistivity, ρ, large saturation induction, B_s, and low coercivity, H_c. In view of these properties optimal results have been obtained on nanogranular films of soft magnetic materials like $(Co_{1-x}Fe_x)$-Al-O, where the excellent magnetic properties of bulk $Co_{1-x}Fe_x$ are combined with the high resistivity of insulating Al-O intergranular layers [2]. Strictly speaking, in a narrow span of nanogranular density these materials open the possibility that ferromagnetic (FM) long-range order (''*magnetic percolation*'') is already *reached*, while ''*physical percolation*'' with the consequence of metallic conductivity is still *absent*. For a long time [3,4] this situation has been termed ''superferromagnetic'' (SFM), synonymous with a collective ferroic magnetic state of single domain ferromagnetic nanoparticles. As a consequence, SFM domains in discontinuous (nonpercolating) granular films are expected to be similar to FM domains in a continuous film, with the decisive difference that the *atomic spins* are replaced by the ''*superspins*'' of the single-domained nanoparticles.

SFM behavior is, however, not expected to occur if FM nanoparticles experience merely dipolar interaction. In the latter case they rather tend to establish dipolar glassy disorder (''superspin glass'', SSG [5,6]) at high packing densities, while SFM ordering necessitates some additional exchangelike internanoparticle interaction [7,8]. Hitherto only mesoscopic SFM correlations have been observed either by neutron scattering [9] or by magnetic force microscopy [10] in appropriate systems. In this Letter we demonstrate for the first time patterns of homogeneously magnetized SFM domains in a nonpercolating discontinuous multilayer of $Co_{80}Fe_{20}$ nanoparticles embedded in glassy Al_2O_3 by magneto-optic contrast at x-ray and visible light wavelengths, respectively. The necessary [3,4,8] FM internanoparticle exchange is very probably mediated by ultrasmall paramagnetic particles deposited between the superspin particles [11].

Discontinuous metal-insulator multilayers (DMIMs) like $[Co_{80}Fe_{20}(t_n)/Al_2O_3(3\ \mathrm{nm})]_m$, $m > 1$, experience a perfect Volmer-Weber growth mode with heterogeneous nucleation under nonwetting conditions as sketched in Fig. 1(a) [12,13]. Preparation by focused ion beam sputter-

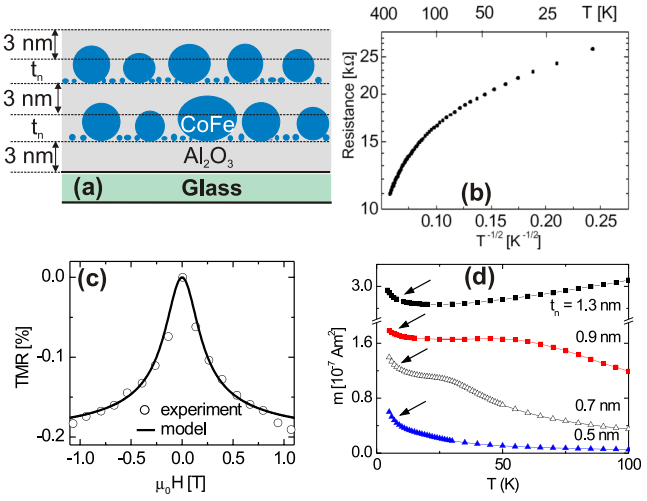

FIG. 1 (color online). (a) Schematic cross section of a discontinuous magnetic-insulator multilayer of $[Co_{80}Fe_{20}(t_n)/Al_2O_3(3\ \mathrm{nm})]_m$. (b) Temperature dependence of electrical resistance R vs $1/T^{1/2}$ and, (c) magnetic field dependence of the CIP tunneling magnetoresistance, TMR, at room temperature for a sample with $t_n = 1.3$ nm and $m = 10$. (d) Temperature dependence of the magnetic moment m^{FC} of $[Co_{80}Fe_{20}(t_n)/Al_2O_3(3\ \mathrm{nm})]_{10}$ with $t_n = 0.5, 0.7, 0.9$, and 1.3 nm, respectively, measured in $\mu_0 H = 10$ mT. Arrows indicate the paramagnetic contributions of the glue particles.

ing allows to control the size $\langle d \rangle$ and the distance $\langle s \rangle$ between the nanoparticles by varying the nominal thickness, t_n, of the magnetic layers at fixed spacer layer thickness, e.g., $\langle d \rangle = 2.8$ nm and $\langle s \rangle \approx 6$ nm for $t_n = 0.9$ nm [6]. Thus the dipolar interaction between the nanoparticles can simply be tuned by controlling t_n [13].

Remarkably, a well-defined magnetic phase diagram of transition temperatures, T_c vs t_n, with different collective states emerges at variant t_n. It comes close to that of dilute magnetic alloys like Au:Fe, which shows first paramagnetism, then a spin glass phase and finally ferromagnetism at increasing Fe concentration [14]. Correspondingly, the DMIM system first shows superparamagnetic (SPM) at $t_n \leq 0.5$ nm, [11] then SSG behavior for $0.5 < t_n < 1.1$ nm, [6] and the SFM state at higher concentrations (1.1 nm $\leq t_n \leq 1.8$ nm) [13]. Finally, percolated three-dimensional ferromagnetism along with Ohmic conduction is encountered in DMIMs above the physical percolation threshold, $t_n \approx 1.8$ nm [12]. Structurally, the atomic spins of conventional magnets are replaced in ''super''magnets (SPM, SSG, and SFM, respectively) by the mesoscopic magnetic moments of nanoparticles (superspins).

While the correspondences between atomic and superparamagnetism on the one hand, and atomic and superspin glass, on the other hand, are straightforward and conceptually simple [5], the equivalence of conventional to superferromagnetism is less evident [13,15]. Systems with purely dipolar interaction reveal ferroic long-range order only in cases, where the nanoparticles register on highly symmetric lattices [16]. Hence, an additional short-ranged exchange interaction is required to stabilize the SFM ground state [4]. Only recently [11] we have found ''glue particles'' being capable of providing a uniform FM interaction between the isolated nanoparticles via FM tunneling exchange [17]. These glue particles are thought to be remainders of the initial coverage during the sputtering process being covered by the subsequent layer of Al_2O_3 before having a chance to reach and merge with the nearest nanoparticle by diffusion processes.

DMIM samples with $t_n = 1.3$ nm and $m = 10$ were prepared by sequential focused Xe-ion-beam sputtering on float glass substrates from high-purity Al_2O_3 and mosaic $Co_{80}Fe_{20}$ targets at constant deposition rates of 0.012 and 0.035 nm/s, respectively. Al_2O_3 top and bottom layers prevent surface oxidation of the CoFe layers. A magnetic field of $m_0H \approx 10$ mT applied during growth parallel to the sample plane gives rise to a well-defined in-plane easy axis. By analysis of FM resonance (FMR) spectra at $T = 300$ K [18] an in-plane uniaxial anisotropy field $H_k \approx 20$ Oe is estimated. The magnetization is measured using a superconducting quantum interference device (SQUID) magnetometer (Quantum Design, MPMS-5S). The electric resistance R vs temperature T was measured in magnetic fields $|B| \leq 1$ T applied along the easy direction at temperatures $5 \leq T \leq 300$ K using two-terminal contacts in current-in-plane geometry. Longitudinal magneto-optical Kerr (LMOKE) microscopy images at spatial resolution of better than 10 μm were recorded at room temperature in weak external magnetic fields parallel to the easy axis. X-ray photoemission electron microscopy (X-PEEM) imaging with a resolution of about 100 nm using the x-ray magnetic circular dichroism at the L_3 absorption edge of Co (778 eV) [19] was performed at the Advanced Light Source in Berkeley, CA, U.S.A.

The bimodal distribution of CoFe particles as depicted in Fig. 1(a) is mirrored by the temperature (T) dependence of the electrical tunneling resistance R of an insulating DMIM sample $[Co_{80}Fe_{20}(1.3\text{ nm})/Al_2O_3(3\text{ nm})]_{10}$. When plotting $\ln R$ versus $T^{-1/2}$ in Fig. 1(b) we do not observe the usual linear relationship, which results from the broad log-normal size distribution of the metallic nanosized granules including the Coulomb blockade effect [20]. The strongly decreasing slope when cooling to low temperatures hints at an increasing dominance of higher order tunneling processes due to the large fraction of extremely small particles [21]. With regard to the possible applications as high-f power management devices we note that the specific resistivity of our sample is fairly high at room temperature, $\rho \approx 1.7 \times 10^4$ $\mu\Omega$ cm, owing to its basic tunneling nature.

As a consequence, the higher order tunneling—in addition to the partial superspin alignment in the remanent state at $H = 0$—gives rise to a fairly small tunneling magnetoresistance (TMR) [21] of only about 0.2% in magnetic fields of $B = 1$ T at room temperature [Fig. 1(c)]. The different magnetic saturation properties of both kinds of granules are reflected by the shape of the TMR curve. A best fit of our data to a recent model theory [22] [full line in Fig. 1(c)] yields reasonable parameters, viz. $m_1 = 5000 \pm 200\mu_B$, $\langle d_1 \rangle = 4.1 \pm 0.5$ nm, and $\mu_2 = 14 \pm 2\mu_B$, $\langle d_2 \rangle = 0.5 \pm 0.1$ nm, for the nano- and the ultrasmall particles, respectively. These numbers comply with those magnetometrically obtained [11].

Figure 1(d) shows the temperature dependence between 5 and 100 K of the magnetic moment of samples $[Co_{80}Fe_{20}(t_n)/Al_2O_3(3\text{ nm})]_{10}$ with comparable areas, but different $t_n = 0.5$, 0.7, 0.9, and 1.3 nm. Upon field cooling in $\mu_0 H = 10$ mT the average moment is monotonically increasing with increasing t_n for a given fixed temperature, roughly in proportion to the total CoFe volume. However, quite different temperature characteristics down to about 25 K mirror the different magnetic natures of the systems involved, being SPM ($t_n = 0.5$ nm) [11], SSG ($t_n = 0.7$ and 0.9 nm) [11], and SFM ($t_n = 1.3$ nm), respectively.

Most importantly, however, the curves have all in common a hyperbolic increase at $T < 25$ K (arrows). This is a clear indication of a paramagnetic component with Curie-type susceptibility response. It does not only occur in SPM ($t_n = 0.5$ nm) [11] and SSG samples ($t_n = 0.7$ and 0.9 nm) [11], but also in the SFM case ($t_n = 1.3$ nm), where novel

FMR data [18] also reveal a distinct paramagnetic nanoparticular subsystem beside the FM one. Interestingly, also FMR clearly reveals two species of nanoparticles, both of which resonate with $g \approx 2.1$ indicating metallic magnetism with essentially quenched orbital moments [18].

The concentration of the isolated quasiatomic paramagnetic particles found to be $n \approx 10^{21}$ cm^{-3}, and, hence, the average distance between the glue particles, $\langle s \rangle \approx 0.5$ nm, was found to be fairly independent of the nominal thickness for $t_n = 0.5$ and 0.7 nm [11]. Inspection of Fig. 1(d) reveals similar numbers for the SFM sample, $t_n = 1.3$ nm. Since the length scale of $\langle s \rangle$ is typical of tunneling processes, we follow the ideas of Kondratyev and Lutz [17], who investigated the tunneling exchange coupling of transition metal dots and their arrays within a band structure based shell model. They stress that the exchange coupling is preferentially FM for large transition metal nanoparticles, but find the same result also for very small Co particles [see Fig. 3(b) in [17]]. We believe this to be relevant for our SFM DMIM, where ferromagnetically polarized chains are established between the nanoparticles [Fig. 1(a)] via tunneling exchange paths.

Figures 2(a)–2(f) shows LMOKE micrographs on the temporal evolution of the switching process at room temperature after saturating the negative magnetization (dark) and, subsequently, exposing the sample to a supercoercive field of $\mu_0 H = 0.65$ mT [see the hysteresis at 300 K in Fig. 2(b) of Ref. [23]]. The first stripelike domains with reversed magnetization (light) appear at time $t \approx 1.5$ s Fig. 2(a). In the next few seconds they are observed to extend simultaneously sideways and along the easy (= field) direction, while further domains nucleate at other sample regions. These sideways *sliding* [15,24] and nucleation processes continue under the same constant field, until all of the down-magnetization is reversed after 9 s. Systematic investigations have shown that the domain nucleation rate and the velocity of subsequent *viscous slide* motion of the walls can accurately be controlled by the magnitude of the external field.

X-PEEM domain images at room temperature with higher resolution are shown in Fig. 3. Spatially and temporally varying magnetic fields of an electrical discharge prepared the sample into a demagnetized state, which shows an equal distribution of up (light) and down magnetized (dark) domains in the absence of an external magnetic field [Fig. 3(a)]. Lamellar domains with an irregular (probably fractal) structure oriented along the easy direction can be observed. The lamellae appear at different

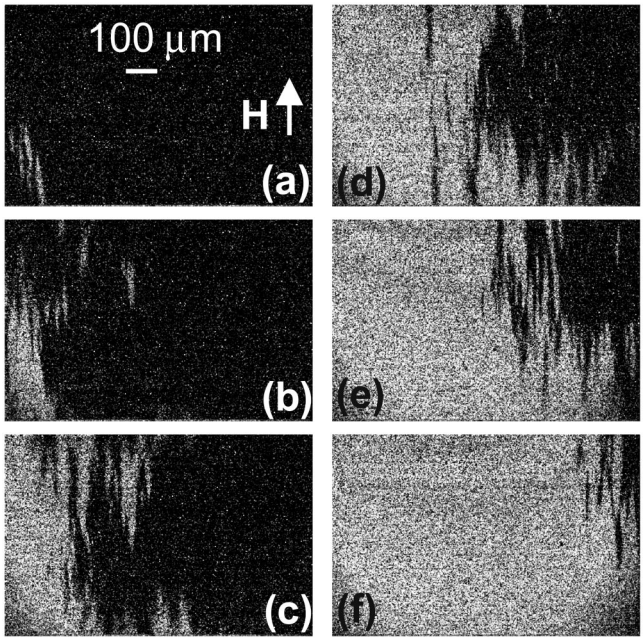

FIG. 2. LMOKE microscopy domain images (980×700 μm^2) of initially remanent $[Co_{80}Fe_{20}(1.3\text{ nm})/Al_2O_3(3\text{ nm})]_{10}$ at room temperature under a supercoercive field, $\mu_0 H = 0.65$ mT, at $t = 1.5$ (a), 2.5 (b), 3.5 (c), 4.5 (d), 5.5 (e), and 7 s (f).

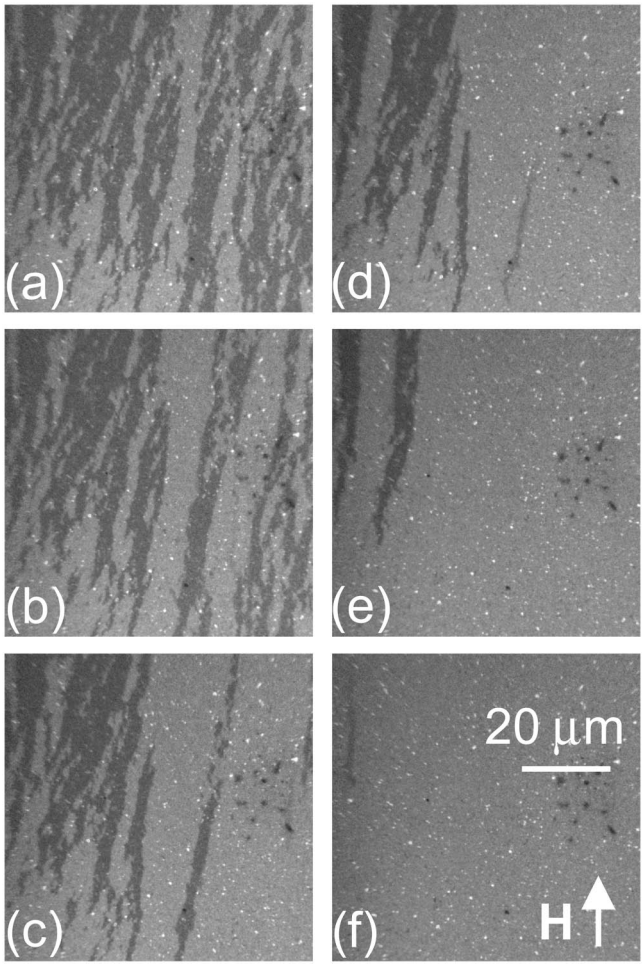

FIG. 3. X-PEEM domain images (70×70 μm^2) of initially demagnetized $[Co_{80}Fe_{20}(1.3\text{ nm})/Al_2O_3(3\text{ nm})]_{10}$ at room temperature under subcoercive fields, $\mu_0 H = 0$ (a), 0.12 (b), 0.14 (c), 0.15 (d), 0.18 (e), and 0.2 mT (f).

length scales and are similar to those shown in Fig. 2; i.e., they show self-similarity and holelike internal structures (''domains in domains'') within the studied length scales between 0.1 and 100 μm. The field-induced evolution of the SFM domains has been probed by sweeping a current through a wire being transversely placed underneath the sample, thus generating subcoercive magnetic fields $0.12 \leq \mu_0 H \leq 0.20$ mT [see the hysteresis at 300 K in Fig. 2(b) of Ref. [23]] along the easy axis. The images in Figs. 3(b)–3(f) (individual exposure time 120 s) show a *creeplike* expansion [24] of the light domains with respect to the dark background as expected in a longitudinal magnetic field, $H < H_c$ [15,23].

Similar irregular domain structures have been observed in hard magnets, e.g., Alnico alloys [25] or $Sm_2Fe_{17}N_3$, [26] consisting of precipitated single domain nanoparticles, which are only weakly exchange coupled across their grain boundaries. It has been argued that these domains are primarily defined by the dipolar stray fields of their constituents, viz., the FM grains or nanoparticles, and were henceforth named ''interaction domains'' [25]. We propose this concept to apply also to our SFM domains, which grow during the magnetization reversal under the constraint of very weak interparticle exchange coupling and dominating dipolar coupling. A reversing opposite magnetic field then tends to cancel the weak exchange field and thus activates the competing forces of the dipolar interaction. At coercivity, the SFM single domain, hence, easily breaks up into antiparallel stripes. This minimizes the magnetostatic energy of the sample (Figs. 2 and 3). It will be interesting to model this SFM scenario with realistic parameters.

Here we state that dipolarly interacting FM nanoparticles can overcome the extreme disorder of the superspin glass state and reveal a novel extremely soft SFM phase provided that they are subject to additional weak FM exchange. The SFM state is single domained in the field range between saturation and remanence as visualized by magneto-optical microscopies. The magnetization reversal is controlled by the interplay of dipolar, exchange, and external magnetic fields involving fuzzy-shaped ''interaction domains.'' As being classic for ferromagnets all along [27], domain visualization has provided strong indication for the long suspected [3,4] SFM state.

Finally, it has to be remarked that magnetic nanoparticles undergoing a transition into the long-range ordered SFM state are clearly unsuitable for applications in data storage, which tries to address independent single particles [28] under blocking conditions beyond the SPM limit [29,30]. Since the remanent SFM alignment counteracts large TMR values [Fig. 1(c)], also magnetic random access memory applications are not promising for DMIMs. However, magnetically ultrasoft SFM materials are nearly ideal candidates for high permeability, low-loss materials for microelectronic, power management, and sensing devices designed for high frequencies [2]. By tuning the nominal CoFe film thickness, viz., granule size and distance, the parameters ρ and H_c can reliably be controlled. Further research has to be devoted to maximize the uniaxial anisotropy field H_k, [2] which is presently controlled by an external field applied during the growth of the DMIMs.

Thanks are due to D. V. Berkov, X. Chen, J. Lindner, Th. Kleinefeld, O. Petracic, and A. Trunova for valuable discussions and to DFG (Graduate School ''Structure and Dynamics of Heterogeneous Systems'' and No. KL306/38) for financial support.

*Corresponding author.
Electronic address: wolfgang.kleemann@uni-due.de

[1] S. Maekawa and T. Shinjo, *Spin Dependent Transport in Magnetic Nanostructures* (Taylor & Francis, London, 2002).
[2] H. Fujimori *et al.*, J. Magn. Magn. Mater. **304**, 32 (2006).
[3] S. Mørup *et al.*, J. Magn. Magn. Mater. **40**, 163 (1983).
[4] D. G. Rancourt and J. M. Daniels, Phys. Rev. B **29**, 2410 (1984).
[5] P. E. Jönsson *et al.*, Phys. Rev. B **64**, 212402 (2001).
[6] S. Sahoo *et al.*, Appl. Phys. Lett. **82**, 4116 (2003).
[7] M. R. Scheinfein *et al.*, Phys. Rev. Lett. **76**, 1541 (1996).
[8] R. Kretschmer and K. Binder, Z. Phys. B **34**, 375 (1979).
[9] S. Sankar *et al.*, J. Magn. Magn. Mater. **221**, 1 (2000).
[10] V. F. Puntes *et al.*, Nat. Mater. **3**, 263 (2004).
[11] X. Chen *et al.*, Phys. Rev. B **72**, 214436 (2005).
[12] G. N. Kakazei *et al.*, J. Appl. Phys. **90**, 4044 (2001).
[13] W. Kleemann *et al.*, Phys. Rev. B **63**, 134423 (2001).
[14] J. A. Mydosh, *Spin Glasses: An Experimental Introduction* (Taylor & Francis, London, 1993).
[15] X. Chen *et al.*, Phys. Rev. Lett. **89**, 137203 (2002).
[16] P. Politi and M. G. Pini, Phys. Rev. B **66**, 214414 (2002).
[17] V. N. Kondratyev and H. O. Lutz, Phys. Rev. Lett. **81**, 4508 (1998).
[18] A. Trunova, S. Bedanta, and J. Lindner (unpublished).
[19] B. Abelès *et al.*, Adv. Phys. **24**, 407 (1975).
[20] J. Stöhr *et al.*, Surf. Rev. Lett. **5**, 1297 (1998).
[21] S. Mitani *et al.*, Phys. Rev. Lett. **81**, 2799 (1998).
[22] C. Wang *et al.*, Phys. Lett. A **329**, 236 (2004).
[23] S. Bedanta *et al.*, Phys. Rev. B **72**, 024419 (2005).
[24] S. Lemerle *et al.*, Phys. Rev. Lett. **80**, 849 (1998).
[25] D. J. Craik and E. D. Isaac, Proc. R. Soc. A **76**, 160 (1960).
[26] W. Rave *et al.*, IEEE Trans. Magn. **32**, 4362 (1996).
[27] P. Weiss, J. Phys. de Rad. **6**, 661 (1907).
[28] S. Sun *et al.*, Science **287**, 1989 (2000).
[29] L. Néel, Ann. Geophys. (C.N.R.S.) **5**, 99 (1949).
[30] W. F. Brown, Jr., Phys. Rev. **130**, 1677 (1963).